{Ag[P(O-*i*-Pr)$_3$]$_3$}BPh$_4$, 89299-17-2; {Ag[P(OPh)$_3$]}BF$_4$, 89299-19-4; {Ag[P(O-*t*-Bu)$_3$]$_2$}BF$_4$, 89299-22-9; {Ag[P(O-*t*-Bu)$_3$]$_2$NO$_3$}, 92054-82-5; {Ag[P(O-*t*-Bu)$_3$]Cl}, 92054-83-6; {Ag[P(O-*t*-Bu)$_3$]CN}, 92054-84-7; {Ag[P(O-2,6-Me$_2$C$_6$H$_3$)$_3$]}BF$_4$, 89299-24-1; MeOPO(CH$_2$)$_2$O, 3741-36-4; MeOPOCH$_2$CMe$_2$CH$_2$O, 1005-69-2; PEt$_3$, 554-70-1; P(OPh)$_3$, 101-02-0; {Ag[P(NMe$_2$)$_3$]$_2$}BPh$_4$, 87883-94-1; [Ag(PEt$_3$)]BF$_4$, 92054-86-9; [Ag(PEt$_3$)$_2$]BF$_4$, 92054-87-0; [Ag(PEt$_3$)$_3$]BF$_4$, 92054-89-2; {Ag[P(OEt)$_3$]}BF$_4$, 92054-90-5; {Ag[P(O-*i*-Pr)$_3$]}BPh$_4$, 92054-92-7; {Ag[P(O-*i*-Pr)$_3$]$_2$}BPh$_4$, 92054-94-9; {Ag[P(O-*t*-Bu)$_3$]}BF$_4$, 92054-96-1; {Ag[P(O-*t*-Bu)$_3$]$_3$}BF$_4$, 92054-98-3; {Ag[P(OCH$_2$CCl$_3$)$_3$]}BF$_4$, 92055-00-0; {Ag[P(OCH$_2$CCl$_3$)$_3$]$_2$}BF$_4$, 92055-02-2; {Ag[P(OCH$_2$CCl$_3$)$_3$]$_3$}BF$_4$, 92055-04-4; {Ag[P(OCH$_2$)$_2$CHO]}BF$_4$, 89299-26-3; {Ag[P(OPh)$_3$]}BF$_4$, 92055-06-6; {Ag[P(OPh)$_3$]$_2$}BF$_4$, 92055-08-8; {Ag[P(O-*o*-tol)$_3$]}BF$_4$, 92055-10-2; {Ag[P(O-*o*-tol)$_3$]$_2$}BF$_4$, 92055-12-4; {Ag[P(O-*o*-tol)$_3$]$_3$}BF$_4$, 92055-13-5; {Ag[P(O-2,6-Me$_2$C$_6$H$_3$)$_3$]$_2$}BF$_4$, 92055-14-6; {Ag[P(O-*t*-Bu)$_3$]$_2$Cl}, 92055-15-7; {Ag[P(O-*t*-Bu)$_3$]$_2$I}, 92055-16-8; {Ag[P(O-*t*-Bu)$_3$]$_3$I}, 92055-17-9; SeP(NMeCH$_2$)$_3$CMe, 68378-99-4; SeP(NMe$_2$)$_3$, 7422-73-3; SePEt$_3$, 21522-01-0; SePMePh$_2$, 23176-17-2; SePPh$_3$, 3878-44-2; SeP(OCH$_2$CCl$_3$)$_3$, 92014-23-8; SeP(O-*t*-Bu)$_3$, 92014-24-9; SeP(OPh)$_3$, 7248-72-8; SeP(O-*o*-tol)$_3$, 28049-19-6; SeP(O-2,6-Me$_2$C$_6$H$_3$)$_3$, 92014-25-0; P(O-2,6-Me$_2$C$_6$H$_3$)$_3$, 52830-49-6.

Contribution from the Anorganisch-chemisches Institut der Universität Zürich, CH-8057 Zürich, Switzerland, and Institut für Reaktortechnik, Eidgenössiche Technische Hochschule Zürich, CH-5303 Würenlingen, Switzerland

Direct Observation of the Ground-State Splitting in d^5 and d^7 Metallocenes by Inelastic Neutron Scattering

ANTON STEBLER,*[1a] ALBERT FURRER,[1b] and JOHN H. AMMETER[1a]

Received November 14, 1983

The splitting of the two lowest orbitally degenerate Kramers doublets in d^5 and d^7 metallocenes has been determined by inelastic neutron scattering spectroscopy at 10 K. The separation is 515 ● 10 cm^{-1} in Fe(C$_5$D$_5$)$_2$X, where X = PF_6^-, AsF_6^-, or I_3^-, and 173 ± 5 cm^{-1} in cobaltocene. The orbital degeneracy of the ground state is lifted under the combined effect of nonaxial ligand field components and spin–orbit coupling. The analysis of the neutron data confirms that the dynamic Jahn–Teller effect has to be taken into account. The vibronic coupling is of comparable importance, resulting in a drastic reduction of the ground-state parameters calculated in an adiabatic model. Several molecular vibrations, particularly of cobaltocene, have been observed by inelastic neutron scattering and IR. By comparison with d^5, d^6, d^7, and d^8 metallocenes, an assignment of frequencies to the fundamental modes of vibration has been performed.

1. Introduction

The dicyclopentadienyl transition-metal complexes, particularly ferrocene, have been the subject of many experimental and theoretical studies since their discovery. Of special interest to the theoretical chemist has been the nature of the unusual chemical bonding of these highly symmetrical sandwich compounds.[2] A very simple electrostatic model[3,4] allows the rationalization of a remarkably large number of properties of the full series of stable metallocenes of the first transition series such as ground-state configurations, trends in the metal–carbon bond lengths, and thermodynamic stabilities.

Ferrocene, the most stable metallocene, is a diamagnetic, closed-shell d^6 system. The remaining members of the first transition series are paramagnetic, where the d^5 and d^7 metallocenes may have a quasi orbitally degenerate ground state. The latter are of particular interest since they may be subject to a Jahn–Teller distortion allowing a deeper insight into their electronic structure. In order to determine quantitative information about chemical bonding and dynamic Jahn–Teller effects in orbitally degenerate sandwich molecules, d^5 and d^7 metallocenes have been diluted in a large variety of diamagnetic host systems and have been studied by EPR.[5-9] The pronounced host lattice dependence of the **g** tensors can be explained almost entirely by changes in the low-symmetry components of the matrix potentials splitting the orbital degeneracy of the guest molecule by different amounts. With use of perturbation theory a strong dependence of the **g** tensor of the ground state on the first excited Kramers doublet can be shown. Thus the separation of the two lowest states can be estimated by EPR experiments.[5-9]

On the other hand, theoretical calculations by Ammeter and Swalen[6] suggest that the splitting between these two states is drastically reduced by the dynamic Jahn–Teller effect compared to the case for the simpler adiabatic model. This reduction is associated with the fact that the upper doublet is energetically much closer to the lowest excited vibrational levels and therefore undergoes a much stronger vibronic mixing effect than the lower doublet. Hence the vibronic coupling suppresses a substantial part of the static rhombic field.

Even though these energy splittings are too large for direct determination by EPR, the splitting of the two lowest Kramers doublets has been estimated to be about 200 cm^{-1} in cobaltocene and, depending on the host lattice, between 500 and 1000 cm^{-1} in the ferrocenium ion.[5-10] Infrared and Raman spectroscopy, which cover the spectral range of interest, suffer in their applicability from the selection rule $\Delta S = 0$.[11]

Inelastic neutron scattering (INS) is a powerful tool for the study of low-energy excitations in crystalline transition-metal and lanthanide compounds.[12-14] Splittings on the order of a few to several hundred wavenumbers are accessible by INS;

(1) (a) Universität Zürich. (b) ETH Zürich.
(2) Warren, K. D. *Struct. Bonding (Berlin)* **1976**, *27*, 45.
(3) Robertson, R. E.; McConnell, H. M. *J. Phys. Chem.* **1960**, *64*, 70.
(4) Nussbaum, M.; Voitländer, J. *Z. Naturforsch., A* **1965**, *20A*, 1411, 1417.
(5) Ammeter, J. H. *J. Magn. Reson.* **1978**, *30*, 299.
(6) Ammeter, J. H.; Swalen, J. D. *J. Chem. Phys.* **1972**, *57*, 678.
(7) Bucher, R. Ph.D. Thesis, Eidgenössische Technische Hochschule Zürich, Zürich, Switzerland, 1977.
(8) Bachmann, J. Ph.D. Thesis, Eidgenössische Technische Hochschule Zürich, Zürich, Switzerland, 1981.
(9) Zoller, L. F. Ph.D. Thesis, University of Zürich, Zürich, Switzerland, 1983.
(10) König, E.; Schnakig, R.; Kremer, S.; Kanellakopulos, B.; Klenze, R. *Chem. Phys.* **1978**, *27*, 331.
(11) Gächter, B. F.; Koningstein, J. A.; Aleksanyan, V. T. *J. Chem. Phys.* **1975**, *62*, 4628.
(12) As in introduction to the method see, e.g.: Bacon, G. E. "Neutron Diffraction"; Clarendon Press: Oxford, England, 1975.
(13) Güdel, H. U.; Stebler, A.; Furrer, A. *J. Phys. C* **1980**, *13*, 3817.
(14) Stebler, A.; Güdel, H. U.; Furrer, A.; Kjems, J. K. *Inorg. Chem.* **1982**, *21*, 380.

0020-1669/84/1323-3493$01.50/0

therefore, we have used this technique to directly determine the splitting of the lowest Kramers doublets in d^5 and d^7 metallocenes.

2. Experimental Section

2.1. Synthesis and Crystal Growth. $Fe(C_5H_5)_2$ and $Fe(C_5D_5)_2$ are commercially available (Merck and Merck Sharp and Dohme, respectively) and were used without further purification. The deuterium content of $Fe(C_5D_5)_2$ was ≥98%.

Literature procedures were used for the preparation of $Fe(C_5H_5)_2I_3$, $Fe(C_5D_5)_2I_3$,[15] $Fe(C_5H_5)_2X$, and $Fe(C_5D_5)_2X$,[16] where X = PF_6^- or AsF_6^-. For the synthesis of $Fe(C_5D_5)_2X$ the procedure was adapted with H_2SO_4 and H_2O replaced by D_2SO_4 and D_2O, respectively. All stoichiometries were confirmed by elemental analysis. The authors are indebted to Dr. A. Salzer of the University of Zürich, Switzerland, for providing samples of $Co(C_5H_5)_2PF_6$, $Co(C_5H_5)_2$, $Co(C_5D_5)_2$, $Ni(C_5H_5)_2$, and $Ni(C_5D_5)_2$.

With use of a temperature gradient furnace single crystals of cobaltocene of up to 150 mm^3 were obtained from a saturated isooctane solution sealed in an ampule. Since cobaltocene is air and moisture sensitive, all handlings were carried out in a drybox.

In a previous X-ray study Bünder and Weiss[17] showed that cobaltocene crystallizes at room temperature in a monoclinic structure with the cyclopentadienyl rings of a molecule parallel to one another in a staggered conformation. Detailed structural studies on ferrocene,[18-21] nickelocene, and ruthenocene[22] suggest a more complicated situation concerning the ring rotation. The low-temperature structure of cobaltocene is unknown.

2.2. Inelastic Neutron Scattering. Due to the large incoherent scattering contribution of ^1H, undeuterated samples are not well suited for the study of magnetic excitations by thermal neutrons. Experiments were therefore performed on polycrystalline $Fe(C_5D_5)_2X$, where X = PF_6^-, AsF_6^-, or I_3^- (degree of deuteration ≥98%), and $Co(C_5D_5)_2$ (degree of deuteration ≥90%). Powdered samples were sealed under helium in aluminum cylinders of 8-mm diameter and 5-cm length. For the single-crystal experiments a cobaltocene crystal was mounted on the spectrometer so that the monoclinic *b* axis was perpendicular to the neutron scattering plane. The final alignment was achieved by neutron diffraction using the reflections (100) and (20$\bar{2}$). With this orientation, the scattering vector $\vec{Q}$ was in the crystallographic a^*c^* plane. For all measurements $\vec{Q}$ was chosen parallel to the a^* axis. The INS experiments were performed at the reactor Saphir in Würenlingen using a triple-axis spectrometer. The measurements were carried out in the constant-$\vec{Q}$ mode of operation in the neutron energy-loss configuration with the analyzer energy kept fixed at 121 cm^{-1}. The resolution was 8 cm^{-1} for the elastic line and increased to about 20 and 40 cm^{-1} for energy transfers of 200 and 400 cm^{-1}, respectively.

2.3. Infrared Spectra. IR spectra between 200 and 700 cm^{-1} of $Fe(C_5H_5)_2PF_6$, $Fe(C_5D_5)_2PF_6$, $Fe(C_5H_5)_2I_3$, and $Fe(C_5D_5)_2I_3$ were obtained with a Perkin-Elmer 983 IR spectrophotometer. CsI pellets were used throughout.

3. Theoretical Section

3.1. Ground State of d^5 and d^7 Metallocenes. In low-spin d^5 and d^7 metallocenes with D_{5d} symmetry the unpaired electron is situated in e_2 and e_1 orbitals, respectively, resulting in an orbitally degenerate $^2E_{2g}$ ground state in d^5 systems and $^2E_{1g}$ in d^7 metallocenes. These degenerate ground states may

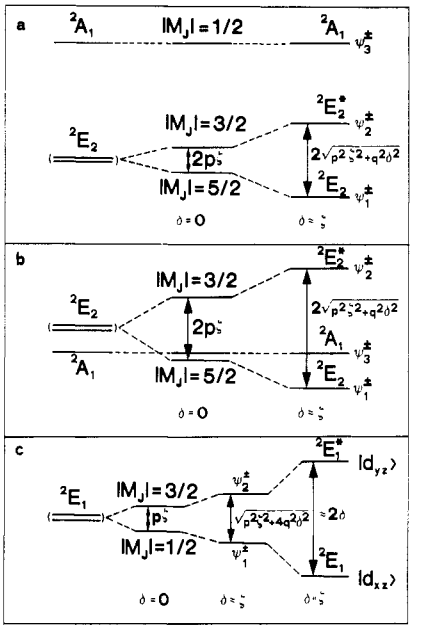

Figure 1. Schematic splitting of low-spin d^5 and d^7 metallocenes with D_{5d} symmetry under the combined effect of spin–orbit coupling and rhombic distortion of the ligand field: (a) ferrocenium ion as in ref 32; (b) ferrocenium ion as in ref 11, 15, 29; (c) cobaltocene. The Kramers doublets of the d^5 system are given by $|\Psi_1^{\pm}\rangle = \cos\xi_2|\phi_2^{\pm}\rangle \mp i\sin\xi_2|\phi_3^{\pm}\rangle$ and $|\Psi_2^{\pm}\rangle = \sin\xi_2|\phi_2^{\pm}\rangle \pm i\cos\xi_2|\phi_3^{\pm}\rangle$ and those of the d^7 metallocenes by $|\Psi_1^{\pm} = \cos\xi_1|\phi_4^{\pm}\rangle \mp i\sin\xi_1|\phi_5^{\pm}\rangle$ and $|\Psi_2^{\pm}\rangle = \sin\xi_1|\phi_4^{\pm}\rangle \pm i\cos\xi_1|\phi_5^{\pm}\rangle$.

split under the combined effect of nonaxial ligand field components δ and spin–orbit coupling ζ. The real LCAO basis functions can be written as

$$\begin{aligned}
|\phi_1\rangle &= c_1|3d_{z^2}\rangle - c_1'|\phi_1^{lig}\rangle && a_{1g}\\
|\phi_2\rangle &= c_2|3d_{x^2-y^2}\rangle - c_2'|\phi_2^{lig}\rangle \\
|\phi_3\rangle &= c_3|3d_{xy}\rangle - c_3'|\phi_3^{lig}\rangle && e_{2g}\\
|\phi_4\rangle &= c_4|3d_{xz}\rangle - c_4'|\phi_4^{lig}\rangle \\
|\phi_5\rangle &= c_5|3d_{yz}\rangle - c_5'|\phi_5^{lig}\rangle && e_{1g}
\end{aligned} \qquad (1)$$

where $c_i^2 + c_i'^2 - 2c_ic_i'S_i = 1$.

The spin–orbit coupling, the static rhombic crystal field, and the Zeeman interaction are described by the Hamiltonian

$$\hat{\mathcal{H}} = \hat{\mathcal{H}}_{so} + \hat{\mathcal{H}}_{rhomb} + \hat{\mathcal{H}}_{ze} \qquad (2)$$

$$= \zeta\hat{l}\cdot\hat{s} + \hat{V}_{rhomb} + \sum_i (k\hat{l} + g_e\hat{s})\beta H_i \quad i = x, y, z \qquad (3)$$

with $\delta = -\langle\phi_4|\hat{V}_{rhomb}|\phi_4\rangle = \langle\phi_5|\hat{V}_{rhomb}|\phi_5\rangle = -\langle\phi_2|\hat{V}_{rhomb}|\phi_2\rangle = \langle\phi_3|\hat{V}_{rhomb}|\phi_3\rangle$. Ammeter and Swalen suggest in their detailed studies[6] that the static molecular orbital (MO) description should be replaced by a model considering the dynamic coupling between electronic and vibrational states. The interaction between nuclear and electronic motions (dynamic Jahn–Teller effect) results in a reduction of certain matrix elements. This reduction may be described by vibronic quenching parameters ("Ham factors"[23]), which approach unity in the adiabatic approximation and zero (V, p) or $^1/_2$ (q) for large linear Jahn–Teller couplings. The vibronic coupling can be expected to influence the splitting of the two nearly degenerate Kramers doublets. As a consequence of the dynamic Jahn–Teller effect there are much smaller spin–orbit coupling and orthorhombic ligand field parameters in comparison to those for the adiabatic description. Furthermore, the orbital reduction factor k is reduced due to vibronic mixing resulting in smaller deviations of $g_{\parallel}$ (parallel to the unique molecular axis) from the free-electron value. On the other hand, dynamic coupling between electronic and vibrational

(15) Hendrickson, D. N.; Sohn, Y. S.; Gray, H. B. *Inorg. Chem.* **1971**, *10*, 1559.
(16) Brauer, G. "Handbuch der präparativen anorganischen Chemie"; F. Enke-Verlag: Stuttgart, West Germany, 1981; Vol. III, p 1845.
(17) Bünder, W.; Weiss, E. *J. Organomet. Chem.* **1975**, *92*, 65.
(18) Takusagawa, F.; Koetzle, T. F. *Acta Crystallogr., Sect. B: Struct. Crystallogr. Cryst. Chem.* **1979**, *B35*, 1074.
(19) Seiler, P.; Dunitz, J. D. *Acta Crystallogr., Sect. B: Struct. Crystallogr. Cryst. Chem.* **1979**, *B35*, 1068, 2020; **1982**, *B38*, 1741.
(20) Clec'h, G.; Calvarin, G.; Bérar, J. F.; Kahn, R. *C.R. Seances Acad. Sci., Ser. C* **1978**, *286*, 315.
(21) Clec'h, G.; Calvarin, G.; Bérar, J. F.; Andrê, D. *C.R. Seances Acad. Sci., Ser. C* **1978**, *287*, 523; *J. Phys. Chem. Solids* **1982**, *43*, 785.
(22) Seiler, P.; Dunitz, J. D. *Acta Crystallogr., Sect. B: Struct. Crystallogr. Cryst. Chem.* **1980**, *B36*, 2255, 2946.
(23) Ham, F. S. *Phys. Rev.* **1965**, *138*, A1727; **1968**, *166*, 307.

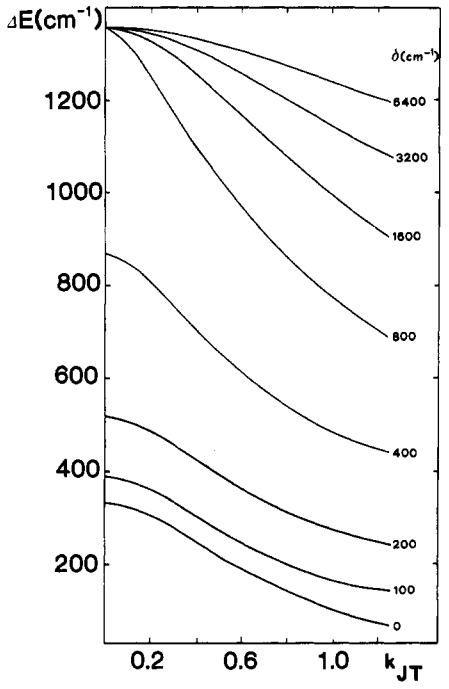

Figure 2. Splitting of the orbitally degenerate ground state ($\Delta E = E_1 - E_2$) as a function of the Jahn–Teller-active coordinate k_{JT} and various orthorhombic distortions calculated from the model of Ammeter and Swalen.[6] All values are strongly dependent on the hypothetical frequency of the Jahn–Teller-active vibration, which is chosen to be 1356 cm^{-1} in this calculation.

states is reduced by increases in the orthorhombic potential. In the extreme case of very large nonaxial components of the ligand field, the electronically labile system passes over to a stereochemically quasi-static one. The two lowest Kramers doublets may then be described by real d orbitals.

In cobaltocene the splitting of the orbitally degenerate ground state under the effects of spin–orbit coupling and an orthorhombic distortion is pictured schematically in Figure 1c. Since the spin–orbit coupling (ζ), the static rhombic crystal field (2δ), and the dynamic Jahn–Teller coupling (k_{JT}) are of comparable importance, the last may not be neglected.[6] The influence of the dynamic coupling on the splitting of the two lowest Kramers doublet is shown in Figure 2. As can be seen, the reduction of the parameters ζ, δ, and ΔE is primarily due to vibronic coupling; therefore, the interplay of spin–orbit coupling, static rhombic distortion, and dynamic Jahn–Teller effect determines the magnetic properties of the ground state and the splitting to the first excited Kramers doublet of the cobaltocene molecule. This reduction is expressed by the Ham type factors p and q. Since the first excited Kramers doublet is only about 150 ± 50 cm^{-1} higher in energy than the ground state,[6,10] a small perturbation of the matrix potential has an observable influence on the magnetic properties of the ground-state doublet. This effect may be taken advantage of by doping cobaltocene in a large variety of diamagnetic host lattices and studying the pronounced dependence of the **g** tensor by EPR.[5-9] Unfortunately undiluted cobaltocene shows only a broad EPR resonance at $g = 1.69$ From susceptibility measurements by Oswald[24] an energy splitting of 330 cm^{-1} was estimated whereas experiments reported more recently by König[10] give a value of 146 cm^{-1}.

The electronic structure of the *ferrocenium ion* has been a subject of continuing interest.[11,15,25-34] EPR studies[31-34] and magnetic susceptibiltiy measurements[15] confirmed that the ferrocenium ion has a $^2E_{2g}$ ($e_{2g}^3\ a_{1g}^2$) ground state, which is split into two Kramers doublets by spin–orbit coupling and crystal fields of low symmetry (Figure 1a,b). This splitting shows a pronounced sensitivity to alkyl substituents on the cyclopentadienyl rings and to changes in the anion.[6,15] Furthermore, there is an excited $^2A_{1g}$ ($e_{2g}^4\ a_{1g}$) state with the unpaired electron in the d_{z^2} orbital. To date there is confusion concerning the energy of this state. From EPR studies of ferrocenium salts the splitting of the two Kramers doublets is estimated to be about 900 cm^{-1}.[31-34] Photoelectron data of ferrocene indicate a $^2A_{1g} \rightarrow E_{2g}$ separation of some 2800 cm^{-1}. Contrary to these results susceptibility[15,29] and Raman[11,30] measurements suggest a much smaller splitting, $\Delta E(^2A_{1g} \rightarrow {}^2E_{2g})$, of approximately 300 cm^{-1}. Although there is no direct correlation of these results, a careful comparison shows that they are incompatible.[8]

In an another attempt to explain magnetic susceptibility data[15] and EPR and magnetic circular dichroism (MCD) experiments[28] a temperature-dependent low-symmetry ligand field parameter was assumed. Later on, this suggestion was ruled out on the basis of the temperature independence of the electronic $^2E_{1u} \leftarrow {}^2E_{2g}$ transition.[27] From a model calculation, with orbital and electron repulsion energies, a splitting of the $^2E_{2g}$ and $^2A_{1g}$ states of approximately 700 cm^{-1} was estimated.[25] Anderson and Rai[29] proposed that the $^2A_{1g}$ level (introduced to explain the susceptibility and MCD data) is not a pure electronic state but a vibronic one of symmetry A_{1g} resulting from Jahn–Teller-induced vibrational coupling with the $^2E_{2g}$ state. Both splitting patterns discussed above are depicted in Figure 1. To data no study has been performed to explain all experimental data simultaneously considering configuration interactions with excited states and the dynamic Jahn–Teller effect. From the experimental point of view the two most important questions are as follows: (1) What are the energy separations between the $^2A_{1g}$ state and the two Kramers doublets from the $^2E_{2g}$ state? (2) What is the energy splitting between the two lowest Kramers doublets originating from the orbitally degenerate $^2E_{2g}$ state?

3.2. Inelastic Neutron Scattering. The magnetic moment of a neutron can interact with the magnetic moment of an electron whereby the neutron gains or loses energy. In these processes the conservation of both energy and momentum has to be obeyed.

In an INS experiment the sample is irradiated by a collimated monochromatic neutron beam and the scattered neutrons are analyzed according to the energy transfer

$$\hbar\omega = \frac{\hbar^2}{2m}(k_0^2 - k_1^2) \tag{4}$$

where m denotes the neutron mass and k_0 and k_1 are the wavenumbers of incoming and scattered neutrons, respectively. Besides the energy transfer, INS provides information on the momentum transfer

$$\hbar\vec{Q} = \hbar(\vec{k}_0 - \vec{k}_1) \tag{5}$$

where $\vec{Q}$ is the scattering vector and $\vec{k}_0$ and $\vec{k}_1$ are the wave

(24) Oswald, N. Ph.D. Thesis, Eidgenösische Technische Hochschule Zürich, Zürich, Switzerland, 1977.
(25) Sohn, Y. S.; Hendrickson, D. N.; Gray, H. B. *J. Am. Chem. Soc.* **1970**, *92*, 3233; **1971**, *93*, 3603.
(26) Hendrickson, D. N.; Sohn, Y. S.; Duggan, D. M.; Gray, H. B. *J. Chem. Phys.* **1973**, *58*, 4666.
(27) Duggan, D. M.; Hendrickson, D. N. *Inorg. Chem.* **1975**, *14*, 955.
(28) Rowe, M. D.; McCaffery, A. J. *J. Chem. Phys.* **1973**, *59*, 3786.
(29) Anderson, S. E.; Rai, R. *Chem. Phys.* **1973**, *2*, 216.
(30) Aleksanyan, V. T.; Haley, L. V.; Koningstein, J. A.; Parameswaran, T. *J. Chem. Phys.* **1977**, *66*, 3835.
(31) Prins, R.; Reinders, F. J. *J. Am. Chem. Soc.* **1969**, *91*, 4929.
(32) Prins, R. *Mol. Phys.* **1970**, *19*, 603.
(33) Prins, R.; Korswagen, A. R. *J. Organomet. Chem.* **1970**, *25*, C74.
(34) Prins, R.; Kortbeek, A. G. T. G. *J. Organomet. Chem.* **1971**, *33*, C33.

vectors of incoming and outgoing neutrons, respectively.

The interactions of the neutrons with the sample can be expressed in terms of the differential neutron cross section. If we consider that the mean radius of the wave function of an unpaired electron is small compared to $1/Q$ (dipole approximation) and deal with unpolarized neutrons and identical, isolated magnetic scattering centers, the inelastic coherent differential cross section is given by[35]

$$\frac{d^2\sigma}{d\Omega\, d\omega} = \left(\frac{\gamma e^2}{m_e c^2}\right)^2 \left[\frac{1}{2} g F(\vec{Q})\right]^2 \exp[-2W(\vec{Q})] \frac{k_1}{k_0} \times \sum_{\alpha}\left[1 - \left(\frac{Q_\alpha}{Q}\right)^2\right] \sum_{\lambda,\lambda'} p_\lambda |\langle\lambda|\hat{S}_1^\alpha|\lambda'\rangle|^2 \delta(\hbar\omega + E_\lambda - E_{\lambda'}) \quad (6)$$

where $\gamma = 1.913$, the neutron magnetic moment in units of the nuclear magneton, λ, λ' = the wave functions of the initial and final electronic levels, E_λ, $E_{\lambda'}$ = energies of the wave functions λ and λ', respectively, p_λ = population of the state λ, $\alpha = x, y, z$, m_e = mass of the electron, $g = [J(J+1) - L(L+1) + S(S+1)]/[2J(J+1)] + 1$ (Landé factor), $F(\vec{Q}) = \langle j_0\rangle + [(g - g_s)/g]\langle j_2\rangle$ (magnetic form factor), and $\exp[-2W(\vec{Q})]$ = the Debye–Waller factor. The remaining symbols have their usual meaning.

The angular momentum operator $\hat{S}_1$ corresponds to an effective spin operator since the orbital angular momentum is only partly quenched.

The Debye-Waller factor is introduced in order to take into account the vibrations of the magnetic ions around the equilibrium position as well as the deviations from the Born–Oppenheimer approximation. In practice, because of line broadening due to relaxation effects and instrumental resolution, the δ function is replaced by a Gaussian.

On the other hand, the following differential neutron cross section for phonon scattering in molecular systems may be derived:

$$\frac{d^2\sigma}{d\Omega\, d\omega} = c\frac{k_1}{k_0}\sum_\nu \left(\frac{\sigma_\nu^{inc}}{M_\nu}\right) \exp[-2W_\nu(\vec{Q})] \sum_{j,\vec{q}} \frac{1}{\omega_j(\vec{q})} |\vec{Q}\cdot \hat{e}_{\nu j}(\vec{q})|^2 [n_j(\vec{q})\, \delta(\omega + \omega_j(\vec{q})) + (n_j(\vec{q}) + 1)\delta(\omega - \omega_j(\vec{q}))] \quad (7)$$

where c is a constant, σ_ν^{inc} the incoherent scattering cross section of nucleus ν, and M_ν the mass of nucleus ν. The first summation extends over all nuclei in the unit cell and the second over the three polarization branches j and the N vectors $\vec{q}$ in the Brillouin zone, where N is the number of unit cells. $\omega_j(\vec{q})$ and $\sum_\nu \vec{e}_{\nu j}(\vec{q})$ are the eigenvalue and eigenvector of the phonon with vector $\vec{q}$ and polarization j. $n_j(\vec{q})$ is the Bose occupation number. The first term in brackets corresponds to absorption and the second to emission of vibrational excitations. From the two differential cross sections (eq 6 and 7) the great advantage of INS compared with other spectroscopic techniques becomes evident since INS is able to unambiguously discriminate between transitions of vibrational and magnetic origin. First, with increasing modulus of the scattering vector $\vec{Q}$ the intensity of vibrational scattering increases approximately as Q^2, whereas for magnetic excitations the intensity of scattered neutrons decreases according to the square of the magnetic form factor $F^2(\vec{Q})$. Second, the temperature dependence of neutrons scattered by phonons is governed by Bose statistics, whereas the intensity of magnetic origin follows the Boltzmann population of the initial state. Third, if a new band is observed after deuteration of the sample, this intensity unambiguously corresponds to a magnetic transition, since the incoherent proton cross section is at least 1 order of magnitude larger than those of any other nucleus.

(35) Marshall, W.; Lovesey, S. W. "Theory of Thermal Neutron Scattering"; Clarendon Press: Oxford, England, 1971.

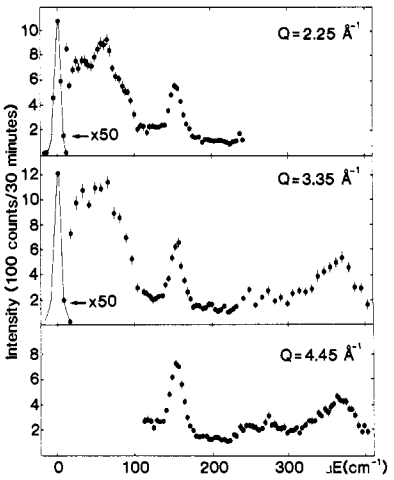

Figure 3. INS spectra of polycrystalline $Co(C_5D_5)_2$ at 10 K. The intense band at zero energy transfer is due to elastic neutron scattering.

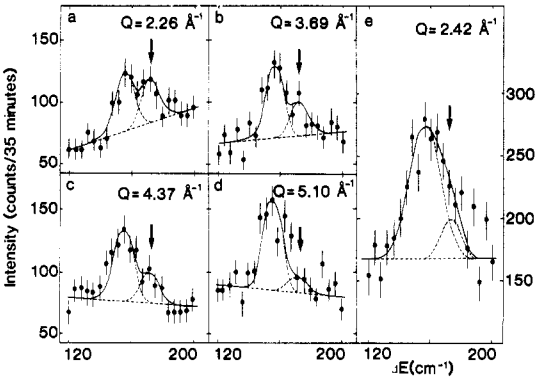

Figure 4. INS spectra of a single crystal of cobaltocene for different moduli of the scattering vector $\vec{Q}$ at 8 K (a–d) and at room temperature (e). $\vec{Q}$ is always parallel to the a^* axis. The curves are the results of a least-squares fit as explained in the text.

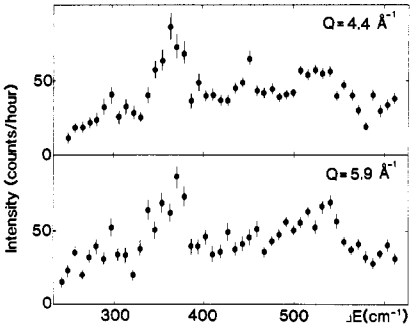

Figure 5. Energy spectra of neutrons scattered from polycrystalline deuterated ferrocene at $T = 8$ K. The intensity near 360 cm^{-1} is due to contamination by higher order Bragg scattering.

4. Results

Figure 3 shows three INS spectra of deuterated polycrystalline cobaltocene at 10 K. The width of the peaks is determined by instrumental resolution. The intensity of the four dominant peaks (155, 249, 275, and 365 cm^{-1}) increases with increasing modulus of the scattering vector $\vec{Q}$. The band at 155 cm^{-1} shows an asymmetric shape diminishing with an increase in $\vec{Q}$. No isolated magnetic peaks were found between 80 and 240 cm^{-1}. Within the experimental accuracy no energy dispersion could be observed.

Single-crystal INS spectra of $Co(C_5H_5)_2$ are given in Figure 4. Between 120 and 200 cm^{-1} two unresolved bands with different $\vec{Q}$ dependences are observed. At 10 K the intensity

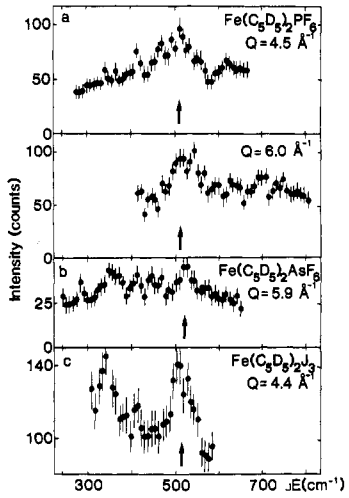

Figure 6. Energy spectra of neutrons scattered from three ferrocenium salts at 8 K: (a) $Fe(C_5D_5)_2PF_6$; (b) $Fe(C_5D_5)_2AsF_6$; (c) $Fe(C_5D_5)_2I_3$.

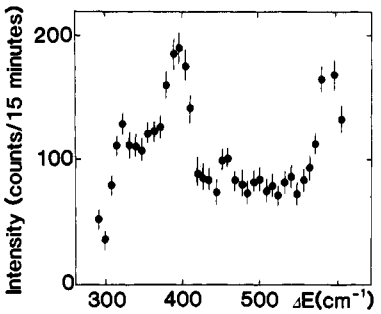

Figure 7. INS spectrum of polycrystalline $Co(C_5H_5)PF_6$ at 10 K. The modulus of the scattering vector $\bar{Q}$ was kept fixed at 4.5 Å^{-1}.

of the band at 157 cm^{-1} rises, whereas the intensity of the peak near 173 cm^{-1} decreases with increasing scattering vector. The intensity and the half-width of the former band become larger with increasing temperature, dominating the spectrum at room temperature.

Figures 5–7 show selected INS powder spectra of deuterated ferrocene, three ferrocenium salts, and $Co(C_5H_5)_2PF_6$, respectively, in the energy range between 200 and 800 cm^{-1}. In addition to the molecular vibrations the INS spectra of ferrocene and the ferrocenium salts display peaks at approximately 520 cm^{-1} with opposite dependence of the intensity upon scattering vector Q. For the cobaltocenium salt there is no peak in that region. The IR frequencies in the low-energy region of $Fe(C_5H_5)_2PF_6$, $Fe(C_5D_5)_2PF_6$, $Fe(C_5H_5)_2I_3$, and $Fe(C_5D_5)_2I_3$ are given in Table I and Figure 8.

5. Discussion

5.1. Assignment of Vibrational Frequencies. Molecular vibration in the low-energy region of d^5, d^6, d^7, and d^8 metallocenes known from IR, Raman, and INS methods are compared in Table I and Figure 8. Most bands observed in this work (Figures 3–7) may be unambiguously assigned to fundamental modes of cobaltocene, ferrocene, and the ferrocenium or cobaltocenium ions.

Deuteration of the cyclopentadienyl rings shifts the vibrational modes to lower energies for ferrocene, the ferrocenium ion, and nickelocene with the exception of the symmetric ring–metal–ring stretching mode (ν_4) of the ferrocenium ion.[36,37] As depicted in Figure 8, d^5 and d^6 metallocenes have

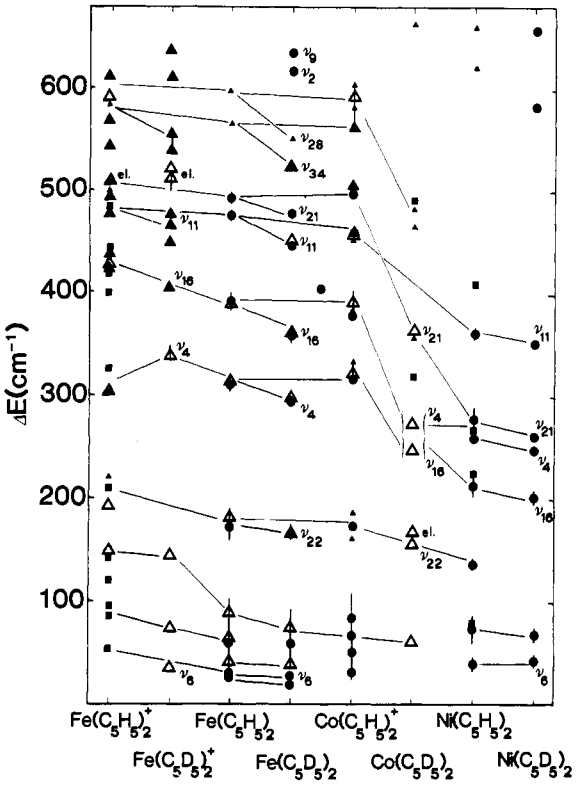

Figure 8. Vibrational frequencies of d^5, d^6, d^7, and d^8 metallocenes of the first transition-metal series lower in energy than 650 cm^{-1}: (open triangles) this work, INS data; (large solid triangles) this work, IR data; (solid circles) data from ref 36, 37, 44, 45; (solid boxes) data from ref 11; (small solid triangles) data from ref 27, 38, 39, 46, 47 (el. = electronic transition $^2E \rightarrow {}^2E^*$).

approximately the same vibrational energies; therefore, the band at ~200 cm^{-1} in the ferrocenium salt spectrum is assigned to the ring–metal–ring bending (ν_{22}). All bands of frequencies lower in energy than 160 cm^{-1} are attributed to lattice modes, contrary to the assignments by Gächter.[11] As one passes from the d^6 to d^7 and d^8 metallocenes the vibrational spectrum changes drastically. Ground-state configurations and electronic states derived from a simple MO model are given in Table II. From this table it is seen that the electrons of d^5 and d^6 metallocenes occupy only bonding orbitals (e_{2g} and a_{1g}), whereas for cobaltocene and for nickelocene there are one and two electrons in the first antibonding orbital (e_{1g}), respectively.

When the ferrocenium ion, ferrocene, and the cobaltocenium ion are compared, no drastic changes of the position of vibrational levels are expected, since the ground electronic configuration involves only bonding orbitals. The occupation of the antibonding e_{1g} orbitals in cobaltocene and nickelocene influences the force field, hence shifts in energy of the vibrational modes are expected and observed in these spectra (Figure 8). In cobaltocene the frequency of the symmetric ring tilt (ν_{16}) changes so strongly that it nearly coincides with the symmetric ring–metal–ring stretching model (ν_4), while in nickelocene it has even a lower energy.[11,36] For this reason there is no unambiguous assignment of the INS bands at ~250 and 275 cm^{-1} in the cobaltocene spectrum. The INS spectrum of the cobaltocenium ion shows a reduction of bands compared to those of ferrocene, in agreement with IR and Raman spectra of ferrocenium salts.[11,27,41,42] The vibrational

(36) Chhor, K.; Lucazeau, G.; Sourisseau, C. *J. Raman Spectrosc.* **1981**, *11*, 183.
(37) Sourisseau, C.; Mathey, Y.; Poinsignon, C. *Chem. Phys.* **1982**, *71*, 257.
(38) Hyams, I. J. *Chem. Phys. Lett.* **1973**, *18*, 399; *Spectrochim. Acta, Part A* **1973**, *29A*, 83.
(39) Kimel'fel'd, Ya. M.; Smirnova, E. M.; Aleksanyan, V. T. *J. Mol. Struct.* **1973**, *19*, 329.
(40) Lippincott, E. R.; Nelson, R. D. *Spectrochim. Acta* **1958**, *10*, 307.
(41) Pavlík, I.; Plecháček, V. *Collect. Czech. Chem. Commun.* **1966**, *31*, 2083.

Table I. Low-Energy Molecular Modes of d^5, d^6, d^7, and d^8 Metallocenes

$Fe(C_5H_5)_2PF_6$		$Fe(C_5D_5)_2PF_6$		$Fe(C_5D_5)_2AsF_6$	$Fe(C_5H_5)_2I_3$[11]	$Fe(C_5D_5)_2I_3$		$Fe(C_5H_5)_2BF_4$[11]	$Fe(C_5H_5)_2$		$Fe(C_5D_5)_2$		$Co(C_5H_5)_2^+$		$Co(C_5H_5)_2$		$Co(C_5D_5)_2$	$Ni(C_5H_5)_2$[36]	$Ni(C_5D_5)_2$[36]	
IR, R	INS	IR, R	INS	INS	IR, R	IR, R	INS	IR, R	IR, R[36]	INS	IR, R[36]	INS	IR, R[37,44,45]	INS	IR, R[11]	INS	INS	IR, R	IR, R	
																		44 47		R_z', A_2
			73		54				59.5 64		55 61			32[i]						
								96	68.5 75 84	~62	65.5 72 79	~72	22 70 80 110	83[i]			62	79 80 82	76	R_x', R_y', E_1 lattice modes
			32						35 42 46.5 50.5 95 104	~41 ~89	35 41 46 49.5 93	~35		45[i] 52[i]				64 87		T_z', A_2 T_x', T_y' E_1
	150		145?		142[b]			120[b]												
220[a]	190							211[d]	167 174 180 189	181	161 167 175	166	174	172[i]		157	155	133 138 143		ν_{22} E_{1u}
								295[d]	307		288							256	245	
304[a]	305?		339 350		325			303 314	311 316 317.5	315	292 297 300	~300	319	315[i] 322			275	262 265[j]	253	ν_4 A_{1g}
								400 419	385 389		352 356		380	394			249	208 209	196 210	
425	427	405			430[c] 440				392 394 401	389	360 362 367	~367						219 220 225[l]		ν_{16} E_{1g}
477		448			484	467			480		445	451	460	458				368	355	ν_{11}, A_{2u}
															320[l]			260		
491		477						510	492		475		499		355[h]		365	275 283 290	265	ν_{21} E_{1u}
568					545[c]	540 555			569[e]		526[f]	528			464[h]			795 803 810	830 850	ν_{34} E_{2u}
	591				612[c]	612?			597[e]		552[f]		585[g] 592[h]	593	490[k] 499[h]			788 812		ν_{28} E_{2g}
									810		620									ν_2 A_{1g}
		637																776		
									817		635		859[g]						585	ν_9 A_{2u}
																		777		
								211 295												
					310															$^2E_{2g} \rightarrow {}^2A_{1g}$ $^2E_{2g} \rightarrow {}^2E_{2g}$
	509		511	523			508									173				

[a] See ref 27. [b] In ref 11 assigned to ν_{22}. [c] This work. [d] In ref 11 suggested as electronic transition. [e] See ref 39. [f] See ref 38. [g] See ref 46. [h] See ref 47. [i] See ref 37. [j] In ref 11 assigned as ν_4. [k] In ref 11 assigned as ν_{21}. [l] See ref 11.

Table II. Electronic Configurations and Ground-State Symmetries of Some Metallocenes

d^5	ferrocenium cation	$(e_{2g})^3(a_{1g})^2$	$^2E_{2g}$
d^6	ferrocene cobaltocenium cation	$(e_{2g})^4(a_{1g})^2$	$^1A_{1g}$
d^7	cobaltocene	$(e_{2g})^4(a_{1g})^2(e_{1g})^1$	$^2E_{1g}$
d^8	nickelocene	$(e_{2g})^4(a_{1g})^2(e_{1g})^2$	$^3A_{2g}$

Table III. Ground-State Properties of Cobaltocene Diluted in Various Host Lattices

host	d-(M–C),[a] Å	k_{JT}[b]	δ-($k_{JT} \neq 0$),[b] cm^{-1}	ΔE-($k_{JT} \neq 0$),[b] cm^{-1}	ΔE_{INS}, cm^{-1}
$Mg(C_5H_5)_2$	2.304[c]	1.21	11	~60	
$Os(C_5H_5)_2$	2.22[d]	1.090	76	~120	
$Ru(C_5H_5)_2$	2.191[e]	1.050[h]	98[h]	158[h]	
$Co(C_5H_5)_2$	2.096[f]	0.89	223	~330	173
$Fe(C_5H_5)_2$	2.33[g]	0.735[h]	420[h]	585[h]	

[a] M–C distance of host molecule. [b] Calculated from EPR data assuming a Jahn-Teller-active mode of 1356 cm^{-1}. [c] See ref 48. [d] See ref 49. [e] See ref 22. [f] See ref 17. [g] See ref 19. [h] See ref 6.

frequencies observed in the INS spectra are in good agreement with those found in IR and Raman studies as illustrated in Figure 8 and Table I.

5.2. Cobaltocene. From the Q dependence of the intensities the four dominant bands in the powder spectra of cobaltocene (Figure 3) can easily be identified as molecular vibrations. The assignment of the observed frequencies to fundamental vibrations was performed by comparison with the well-known spectra of $Fe(C_5D_5)_2$ and $Ni(C_5D_5)_2$,[36] which are depicted in Figure 8 and Table I. The ring–metal–ring bending (δ(Cp–M–Cp), ν_{22}) dominates the spectra of both the polycrystalline sample and the single crystal between 120 and 200 cm^{-1}, where the magnetic transition $^2E_{1g} \rightarrow {}^2E_{1g}{}^*$ is most likely to occur. Fortunately, from the dependence of the intensities upon scattering vector and temperature, the unresolved bands observed in the single-crystal spectra of Figure 4 can be unambiguously assigned. The unresolved bands were fitted with the assumption of a linear background and approximation of the peaks by Gaussians. The results of the least-squares fitting procedure are shown as solid curves in Figure 4, whereas the broken curves indicate the background level and the subdivision into individual bands. The band at 157 cm^{-1} is of vibrational origin, since its intensity increases with both increasing scattering vector and temperature. On the other hand, the band at 173 cm^{-1} can be identified as a magnetic transition, because its intensity decreases with $F^2(Q)$ and diminishes with increasing temperature according to Boltzmann statistics, in agreement with eq 6. It is reasonable to attribute the band of magnetic origin to the transition within the two split Kramers doublets. Our result is in good agreement with the energy splitting derived from the susceptibility measurements by König[10] but differs from that reported by Oswald.[24] The metal–ring distance, the Jahn–Teller radius k_{JT}, the distortion parameter $\delta(k_{JT} \neq 0)$, and the energy splitting of cobaltocene diluted in various diamagnetic host lattices are collected in Table III. The parameters k_{JT} and $\delta(k_{JT} \neq 0)$ were obtained from a fit of experimental EPR data using the model developed by Ammeter and Swalen.[6,24] With use of the susceptibility data obtained by Oswald[24] a splitting of the Kramers doublets of 330 cm^{-1} was estimated. A comparison with the INS results shows that the calculated energy separations are overestimated. As discussed in part 3.1 the Jahn–Teller coupling parameter, k_{JT}, and the distortion parameter, δ, may be calculated by diagonalizing the vibronic Hamiltonian in a reduced Born–Oppenheimer approximation, if the frequency of the Jahn–Teller-active coupling mode is known. With a reduction of this frequency k_{JT} increases rapidly, while the low-symmetry component of the ligand field undergoes a moderate decrease.[5-9,24] Thus, our INS experiments provide further evidence that the ring distortion at ~600 cm^{-1} must be mainly responsible for the Jahn–Teller effect rather than the C–C stretching mode at ~1350 cm^{-1}.

Since no INS band shows any energy dispersion, the Co$(C_5H_5)_2$ molecules exist mostly as isolated units, as expected from X-ray structural data;[17] on the other hand, for the cobaltocenium salts doped in layered lattices an energy dispersion of the antisymmetric ring tilt (ν_{21}) has been observed.[37]

5.3. Ferrocene and Ferrocenium and Cobaltocenium Salts. In deuterated ferrocene the peak at 528 cm^{-1} (Figure 5) increases in intensity with increasing modulus of the scattering vector $\vec{Q}$, suggesting an assignment to a vibrational mode. Considering the energy shift upon deuteration of the cyclopentadienyl rings, this INS band may be assigned to the ring deformation ν_{34}.[38,39] The isotopic ratio ρ of 1.08 is in good agreement with the value reported for out-of-plane ring distortions.[40]

The band observed at 510 cm^{-1} in $Fe(C_5D_5)_2PF_6$, $Fe(C_5H_5)_2PF_6$, and $Fe(C_5D_5)_2I_3$ and the band at 520 cm^{-1} in $Fe(C_5D_5)_2AsF_6$ are attributed to an electronic transition since the intensity decreases with increasing $\vec{Q}$ (Figure 6). The INS spectra of the isomorphous cobaltocenium ion[43] (Figure 7) show no band between 500 and 550 cm^{-1} supporting this assignment since as outlined above d^5 and d^6 metallocenes have similar frequencies.

The mean value of 515 ± 5 cm^{-1} corresponds neither to the energy splitting of the $^2E_{2g}$ and $^2A_{1g}$ levels as suggested from Raman[11] and susceptibility measurements[15,29] (~300 cm^{-1}) nor to the separation of the two lowest Kramers doublets as estimated from EPR measurements[29,32] (~900 cm^{-1}). Considering the orbitally degenerate ground state of the ferrocenium ion (D_{5d} symmetry), a considerable Jahn–Teller coupling is anticipated,[6-9] hence a significant reduction of both the $^2E_{2g}$–$^2A_{1g}$ and $^2E_{2g}$–$^2E_{2g}{}^*$ splitting is expected compared to that for an adiabatic model. Since Raman,[11] susceptibility,[15,29] and EPR results[32] have been interpreted in a model neglecting vibronic mixing and configuration interactions, they should be considered with caution. Hence, the magnetic INS bands of the ferrocenium salts at 515 ± 5 cm^{-1} are attributed to the transition within the Kramers doublets of the split $^2E_{2g}$ ground state. Intensity calculations of the $^2E_{2g}$–$^2E_{2g}{}^*$ and the $^2E_{2g}$–$^2A_{1g}$ transition strongly support this assignment (vide infra). In agreement with EPR studies[7] only a weak dependence of the $^2E_{2g}$–$^2E_{2g}{}^*$ splitting on the anion is observed. With use of the adiabatic approximation ($p = q = 1$) and a spin–orbit coupling of 330 cm^{-1} from EPR, a δ value of approximately 275 cm^{-1} is calculated.[7,31,32] Unfortunately, our data are not sufficient to independently determine p, q, and δ, but the INS results stress that neither the adiabatic approximation ($\Delta E \approx 900$ cm^{-1}) nor a dominating vibronic mixing ($p \approx 0$, $q = {}^1/_2$, $\Delta E \approx 275$ cm^{-1}) describes adequately the separation of the two lowest Kramers doublets. Taking into account that p and q depend on each other,[23] choosing a ζ value of 330 cm^{-1}, and using $\Delta E(^2E_{2g}$–$^2E_{2g}{}^*) = 515$ cm^{-1} from the INS experiments,

(42) Pavlík, I.; Klikorka, J. *Collect. Czech. Chem. Commun.* **1965**, *30*, 664.
(43) Bernstein, T.; Herbstein, F. H. *Acta Crystallogr., Sect. B: Struct. Crystallogr. Cryst. Chem.* **1968**, *B24*, 1640.
(44) Mathey, Y.; Clement, R.; Sourisseau, C.; Lucazeau, G. *Inorg. Chem.* **1980**, *19*, 2773.
(45) Sourisseau, C.; Forgerit, J. P.; Mathey, Y. *J. Phys. Chem. Solids* **1983**, *44*, 119.
(46) Hartley, D.; Ware, M. J. *J. Chem. Soc. A* **1969**, 138.
(47) Fritz, H. P.; Schneider, R. *Chem. Ber.* **1960**, *93*, 1171.
(48) Bünder, W.; Weiss, E. *J. Organomet. Chem.* **1975**, *92*, 1.
(49) Jellinek, F. *Z. Naturforsch., B: Anorg. Chem., Org. Chem., Biochem., Biophys., Biol.* **1959**, *14B*, 737.

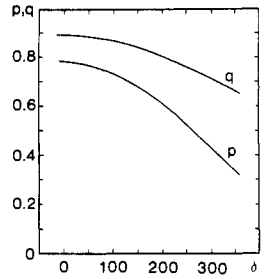

Figure 9. Calculated reduction factors p and q for the $^2E_{2g}$ ground state of the orbital doublet with linear Jahn–Teller coupling, as a function of δ with $q = {}^1/_2(1 + p)$, $\zeta = 330$ cm^{-1}, and $\Delta E(E_{2g}–E_{2g}^*) = 515$ cm^{-1}.

we can calculate p and q as a function of δ (Figure 9). In any case both p and q are significantly higher than in the case of cobaltocene, in agreement with the expectation of a weaker Jahn–Teller coupling in d^5 systems than in d^7 metallocenes.[5,6]

The INS spectrum of $Fe(C_5H_5)_2PF_6$ shows no additional peak between 200 and 400 cm^{-1} which could be assigned to a transition from the ground Kramers doublet ($^2E_{2g}$) to the suggested $^2A_{1g}$ level. The intensity ratio of the INS transitions $^2E_{2g} \rightarrow {}^2E_{2g}^*$ and $^2E_{2g} \rightarrow {}^2A_{1g}$ have been estimated for two limiting cases in the LCAO basis (eq 1) with neglect of the spreading of the spin density onto the ligands ($c_1 = c_2 = c_3 = 1$), the admixture of ligand functions ($c_1' = c_2' = c_3' = 0$), and contributions of the $^2A_{1g}$ state into the ground state.[28] Assuming axial symmetry ($\zeta \neq 0$, $\delta = 0$), the $^2E_{2g} \rightarrow {}^2A_{1g}$ transition is forbidden whereas $^2E_{2g} \rightarrow {}^2E_{2g}^*$ is allowed. If $\delta >> \zeta$, the transition $^2E_{2g} \rightarrow {}^2A_{1g}$ is theoretically half as intense as the $^2E_{2g} \rightarrow {}^2E_{2g}^*$ transition. The intensity ratio of the $Fe(C_5H_5)_2^+$ ion will be still smaller since this d^5 metallocene is situated between the two limiting cases. These results suggest that it would be difficult to locate the $^2A_{1g}$ state by INS. It is hoped that interpretation of the Raman and susceptibility data using an adequate model confirms these conclusions.

Acknowledgment. This work was supported by the Swiss National Science Foundation (Grant No. 2.442.-0.82).

Registry No. $Fe(C_5H_5)_2PF_6$, 11077-24-0; $Fe(C_5D_5)_2PF_6$, 91760-21-3; $Fe(C_5D_5)_2AsF_6$, 91760-22-4; $Fe(C_5H_5)_2I_3$, 1291-35-6; $Fe(C_5D_5)_2I_3$, 91760-23-5; $Fe(C_5H_5)_2BF_4$, 1282-37-7; $Fe(C_5H_5)_2$, 102-54-5; $Fe(C_5D_5)_2$, 12082-87-0; $Co(C_5H_5)_2$, 1277-43-6; $Co(C_5D_5)_2$, 68011-62-1; $Ni(C_5H_5)_2$, 1271-28-9; $Ni(C_5D_5)_2$, 51510-35-1; $Fe(C_5H_5)_2^+$, 12125-80-3; $Co(C_5H_5)_2^+$, 12241-42-8.

Contribution from the Department of Chemistry and Chemical Physics Program, Washington State University, Pullman, Washington 99164-4630

Forbidden Vibrational Modes in Iron(II), Ruthenium(II), and Osmium(II) Hexacyanides: A Tunneling, IR, and Raman Spectroscopy Study

K. W. HIPPS,* STEPHEN D. WILLIAMS, and URSULA MAZUR

Received December 20, 1983

Two of the optically forbidden vibrational fundamentals of the iron-group hexacyanides were directly observed by inelastic electron tunneling spectroscopy. Assignments for these modes in the case of iron(II) hexacyanide are based on their positions, isotopic shifts, and agreement in position of observed bands with those calculated by using an extensively applied valence force potential. Assignments of the optically forbidden modes in the cases of ruthenium and osmium are made by comparing IETS positions and intensities with those observed in the case of iron. Our results support and extend much of the previous work on hexacyanides of the iron-group metals. Some of our assignments for osmium(II) and ruthenium(II) hexacyanides, based on tunneling and polarized Raman data, differ from those previously suggested. One important aspect of this paper is the general observation that tunneling spectroscopy can be used to provide information that is not directly available from Raman and IR studies. Further, IETS lines are somewhat narrower than solution-phase Raman lines. Thus, tunneling spectroscopy is an important new technique complementary to Raman and IR spectroscopy.

Introduction

Understanding the forces that produce molecules from atoms is one of the primary goals of modern inorganic chemistry. These forces are most commonly and easily studied by vibrational spectroscopy. The observed frequencies of fundamental vibrations can be directly related to the forces that hold the molecule together near its equilibrium geometry. Analysis of overtone and combination bands can extend this information to regions somewhat distant from the equilibrium configuration. The analysis of these vibrational data yields force constants that are determined by, and provide information about, the electronic structure of molecules. The methods by which this analysis is performed are well-known and have been extensively applied in inorganic chemistry.[1–4] The primary experimental tools, to date, have been IR and Raman spectroscopy.

While IR and Raman methods have provided a rich yield of information about forces in inorganic systems, they are intrinsically limited by the selection rules that govern the absorption and scattering of light. For example, of the 13 fundamental frequencies of a metal hexacyanide ion, 6 are Raman active, 4 are IR active, and 3 are inactive in both IR and Raman. Thus, a significant portion of the ion's spectrum and the corresponding information about molecular forces are not directly available to the optical spectroscopist. Further, this situation is not unique to the case of octahedral ions. Even for systems of relatively low symmetry (such as C_{3v}), optically inactive bands occur. While these forbidden bands may be observed as combinations or overtones and have frequently been assigned in this manner, these assignments are often ambiguous.

A new vibrational spectroscopy, complementary to IR and Raman but governed by different selection rules, is clearly

* To whom correspondence should be addressed at the Department of Chemistry.

(1) Jones, L. H. "Inorganic Vibrational Spectroscopy"; Marcel Dekker: New York, 1971; Vol. 1.
(2) Adams, D. M. "Metal-Ligand and Related Vibrations"; Edward Arnold: London, 1967.
(3) Nakamoto, K. "Infrared and Raman Spectra of Inorganic and Coordination Compounds", 3rd ed.; Wiley: New York, 1978.
(4) Wilson, E. B.; Decius, J. C.; Cross, P. C. "Molecular Vibrations"; Dover Publications: New York, 1955.

0020-1669/84/1323-3500$01.50/0